Radiated energy from the mid Niigata, Japan, earthquake of October 23, 2004, and its aftershocks

Y. Izutani

Department of Civil Engineering, Shinshu University, Nagano, Japan

[1]   The Mid Niigata earthquake of October 23, 2004, is a shallow reverse-faulting event with M_w = 6.6. We analyze transverse component accelerograms of the main shock and four aftershocks (M_w = 4.0 ∼ 5.5) recorded at 29 strong motion observation stations. The epicenters of the four aftershocks are located within 5 km from that of the main shock. The stations are well distributed around the epicenters and their epicentral distances are between 15 and 60 km. We calculate spectral ratio between records of the main shock and each of the aftershocks in order to obtain source spectral ratio by empirically removing the effects of wave propagation path and surface layers at the stations. Thus obtained source spectral ratio is inconsistent with that expected from the self-similar omega-square model. Fitting omega-square source spectral ratio with variable corner frequency to the observed spectral ratio, radiated energy and corner frequency are estimated. Radiated energy from the main shock is 3.2 × 10^{14} J. Although energy-to-moment ratios for the main shock and the aftershocks are all distributed within a narrow range from 8 × 10^{-6} to 4 × 10^{-5}, they definitely increase with the event size. This scale dependence is quite similar to that obtained previously for strike-slip events in Japan. The relationship between the seismic moment, M_0, and the corner frequency, f_0, is $M_0 \propto f_0^{-3.3\pm0.2}$. These results suggest a break in self-similarity.   **Citation:** Izutani, Y. (2005), Radiated energy from the mid Niigata, Japan, earthquake of October 23, 2004, and its aftershocks, *Geophys. Res. Lett.*, *32*, L21313, doi:10.1029/2005GL024116.

1.   Introduction

[2]   Scaling of earthquake source parameters with size, tectonic environments, and other factors that may influence the rupture process is a very important issue. One of the approaches to this issue is to investigate scale-dependence of seismic energy-to-moment ratio, $\tilde{e} = E_R/M_0$, for earthquakes of various size which occurred in various tectonic regions.

[3]   Mid Niigata earthquake of October 23, 2004, (M_w = 6.6) occurred in the central part of Japan (see Figure 1). This earthquake is a shallow reverse-faulting event. Reverse-faulting is one of the two typical focal mechanisms (strike-slip-faulting and reverse-faulting) for shallow earthquakes in Japan. It was followed by more aftershocks than is normally expected for an $M_w \sim 6$ earthquake in Japan. The epicenters of these earthquakes are well surrounded by stations of strong motion observation networks (K-NET and KiK-net) operated by National Research Institute for Earth

Science and Disaster Prevention, Japan (NIED). Therefore, there are a large quantity of high quality close-in records for these earthquakes.

[4]   Corrections for the attenuation along the wave propagation path, amplification by the surface layers at stations, and the effect of radiation pattern are necessary for estimating the radiated seismic energy, E_R. One of the most reliable methods for estimating E_R is the empirical Green's function (EGF) method [e.g., *Hough and Kanamori*, 2001; *Izutani and Kanamori*, 2001; *Venkataraman et al.*, 2002; *Ide*, 2003]. Taking spectral ratio between two events whose hypocenters are very close to each other and the focal mechanisms are similar, we can in effect remove the path effect, the regional site effect, and the radiation pattern effect. Averaging the spectral ratios at stations well surrounding the epicenters of the events, the directivity effect due to rupture propagation along the fault would be averaged out. The present dataset is very useful for accurate estimation of E_R by the EGF method.

2.   Data and Analysis

[5]   Table 1 lists the main shock (Event 1) and its four aftershocks (Event 2 ∼ 5). These aftershocks have been chosen for the following reasons: (1) Epicenter is located within 5 km from that of the main shock. (2) Focal mechanism is similar to that of the main shock. (3) Focal mechanism and M_0 have been determined with high accuracy by F-net, the broad-band seismometer network operated by NIED. (4) Accelerograms are recorded at more than 15 stations and the azimuthal coverage around the epicenters by of the stations is good.

[6]   Figure 1a shows the location of epicenter of the main shock. Figure 1b shows the locations of the epicenters of the main shock (star) and the aftershocks (solid circles), and the strong motion observation stations (triangles). Figure 1c shows the focal mechanism solutions for the five events by F-net. The stations are located between 15 km and 60 km from the epicenter of the main shock. Actually, there are three stations within 15 km, but their records are not used in the present study. The distance between the hypocenters must be small in comparison with the epicentral distance to the stations in order to satisfy the condition for the EGF method. Besides, the response of surface layers during strong shaking by the main shock may be different from that during weak shaking by the aftershocks because of nonlinear characteristics of surface layers [e.g., *Izutani*, 2004]. In such a case, the response of surface layers is hardly removed by taking the spectral ratio between records.

[7]   The method of analysis used here is almost the same as that used by *Izutani and Kanamori* [2001]. We analyze
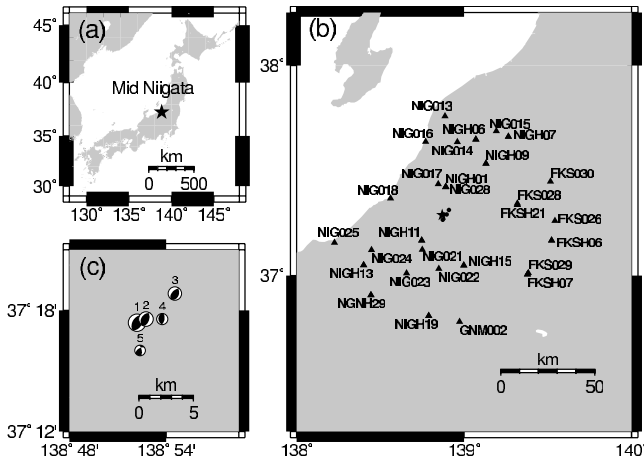
Figure 1. (a) Location of epicenter of the Mid Niigata earthquake. (b) Locations of epicenters of the main shock (star) and the four aftershocks (solid circles), and the K-NET and KiK-net stations (triangles). (c) Focal mechanism solutions for the main shock (Event 1) and the four aftershocks (Event 2 ∼ 5).

the transverse component records obtained by rotating the two horizontal components. We windowed 60-sec long records from the first P-wave arrival. Since S-wave is dominant on the transverse component, the Fourier spectra obtained from the records are regarded as S-wave spectra of transverse component ground acceleration. We take the spectral ratio between Fourier spectra of the main shock and one of the aftershocks to obtain source spectral ratio by removing the effects of radiation pattern, path and site. However, thus obtained spectral ratios show variation from site to site as can be seen in Figure 2. This variation is due to some factors which are not perfectly removed by the above procedure, such as the directivity effect, effects of the small difference in focal mechanisms and the small difference in hypocenter locations. Assuming that influence of these factors is removed by taking average of logarithmic amplitudes of the spectral ratios at stations well distributed around the epicenters, we regard the average spectral ratio as the source spectral ratio.

[8] Theoretical source spectrum, $\dot{M}(f)$, is assumed to have ω^{-2} fall-off above the corner frequency, f_0, [Aki, 1967; Brune, 1970] as

$$\dot{M}(f) = \frac{M_0}{1 + (f/f_0)^2}. \tag{1}$$

According to the result by *Izutani and Kanamori* [2001], the assumption of ω^{-2} fall-off is reasonable for events of the magnitude range in the present study.

[9] The averaged spectral ratio of the records is compared with the ratio of theoretical source spectra,

$$\frac{\dot{M}_1(f)}{\dot{M}_i(f)} = \frac{M_{01}\left[1 + (f/f_{0i})^2\right]}{M_{0i}\left[1 + (f/f_{01})^2\right]}, \tag{2}$$

where the suffixes 1 and $i (i = 2 \sim 5)$ stand for the main shock and one of the aftershocks. The values of M_0 by F-net is adopted because the ground acceleration data analyzed in the present study do not have enough signal-to-noise ratio in the low frequency range to determine M_0 with sufficient accuracy. Fitting theoretical spectral ratio to the observed ones, the corner frequencies for the five events are estimated simultaneously. Then radiated seismic energy, E_R, is evaluated by integrating the theoretical source spectra with the corner frequencies obtained above as

$$E_R = \frac{4\pi}{5\rho\beta^5} \int_0^\infty \left|f\dot{M}(f)\right|^2 df, \tag{3}$$

where ρ is the density and β is the S-wave velocity in the source region, and they are assumed to be the same value ($\rho = 2.7$ g/cm^3 and $\beta = 3.3$ km/sec) used by *Izutani and Kanamori* [2001]. The contribution of P-wave to the radiated energy is assumed to be about 7% of the total radiated energy and E_R obtained by Equation (3) is multiplied by 1.07 [*Mayeda et al.*, 2005].

3. Result

[10] The solid curves in Figure 2 show spectral ratios of the records. The theoretical source spectral ratio expressed by Equation (2) approaches M_{01}/M_{0i} in the low-frequency range and $M_{01}f_{01}^2/M_{0i}f_{0i}^2$ in the high-frequency range. Therefore, the corner frequencies are constrained not only by the frequency at corners of the spectral ratio but also the amplitude of the spectral ratio in the high-frequency range. If large and small earthquakes are similar as assumed by *Aki* [1967],

$$M_0 \propto f_0^{-3} \tag{4}$$

is expected. Therefore the high-frequency source spectral ratio for the self-similar omega-square model, $M_{01}f_{01}^2/M_{0i}f_{0i}^2$,

Table 1. List of Earthquakes and Results of This Study[a]

Event	Date, y m d h m	Latitude, N	Longitude, E	Depth, km	M_w	Strike, deg	Dip, deg	Rake, deg	M_0, Nm	E_R, J	$\tilde{e}$, $\times 10^{-5}$	f_0, Hz	N
1	2004 10 23 17 56	37.290	138.870	13	6.6	212	47	93	7.53×10^{18}	3.2×10^{14}	4.2	0.14	29
2	2004 10 23 19 46	37.293	138.879	12	5.5	217	40	107	1.78×10^{17}	2.8×10^{12}	1.6	0.36	28
3	2004 10 23 23 34	37.314	138.909	19	5.0	223	55	106	4.14×10^{16}	1.2×10^{12}	2.9	0.71	22
4	2004 10 24 16 06	37.293	138.896	12	4.3	174	33	78	3.31×10^{15}	3.0×10^{10}	0.91	1.1	16
5	2004 10 27 00 56	37.267	138.873	13	4.0	238	56	148	1.23×10^{15}	1.6×10^{10}	1.3	1.8	21

[a]Date (Japan Standard Time. GMT+9h) and hypocenter location: after Japan Meteorological Agency. M_w, focal mechanism, and M_0: after National Research Institute for Earthquake Science and Disaster Prevention, Japan (NIED). E_R, $\tilde{e}$, and f_0: results of this study. N: number of stations whose records are used to estimate E_R, $\tilde{e}$, and f_0.
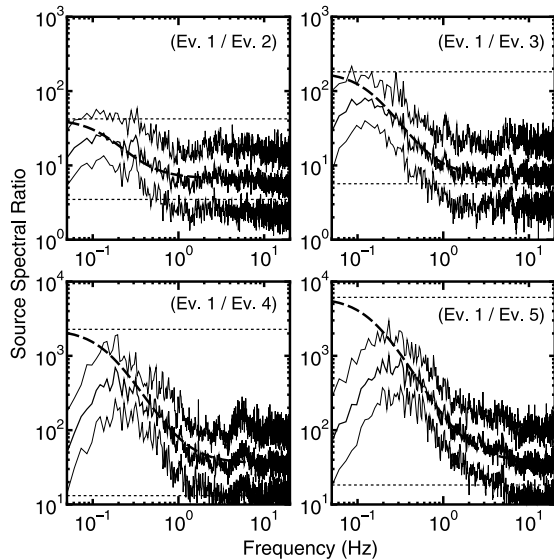
Figure 2. Spectral ratio. The middle solid lines show average spectral ratios of the records at all stations. The upper and lower solid lines show average $\pm$ one standard deviation. The dashed curves indicate best fit theoretical source spectral ratios expressed by Equation (2).

Figure 4. Relationship between seismic moment, M_0, and corner frequency, f_0. The thin dotted lines indicate $M_0 \propto f_0^{-3}$ and the thick dashed line indicates $M_0 \propto f_0^{-3.3}$.

becomes $(M_{01}/M_{0i})^{1/3}$. The upper and lower dotted lines in Figure 2 show M_{01}/M_{0i} and $(M_{01}/M_{0i})^{1/3}$, respectively.

[11] The observed spectral ratios for the four event pairs do not approach M_{01}/M_{0i} in the low frequency range but decrease with decreasing frequency. The frequency below which the observed spectral ratio decreases becomes higher as the magnitude of the aftershocks becomes smaller. The frequency below which the record is contaminated by low-frequency noise becomes higher with decreasing the amplitude of the signal. Therefore, the fall-off of the spectral ratio in the low-frequency range is regarded as the phenomenon caused by the low-frequency noise contaminating the records of the aftershocks.

[12] The spectral ratios of the records are larger than $(M_{01}/M_{02})^{1/3}$ in the high-frequency range, which suggests a break in self-similarity. f_{01} is too large or f_{0i} is too small in comparison with the expectation from the similarity. The
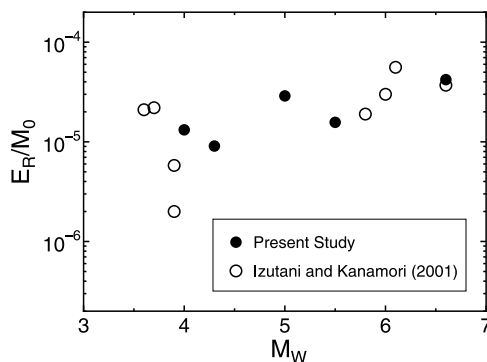
dashed curves indicate the best fit source spectral ratios calculated by Equation (2). The theoretical source spectral ratios fit the observations fairly well. Optimal values for E_R and f_0 are estimated and listed in Table 1.

[13] Figure 3 shows the seismic energy-to-moment ratio, $\tilde{e}$, plotted against M_w. Although all of $\tilde{e}$ for the five events are distributed within a very narrow range between 8×10^{-6} to 4×10^{-5}, they obviously increase with M_w. This scale-dependence of $\tilde{e}$ is almost the same as that found for shallow strike-slip earthquakes which occurred in Japan [*Izutani and Kanamori*, 2001].

[14] Figure 4 shows relationship between M_0 and f_0. The present result and the result by *Izutani and Kanamori* [2001] are plotted together in Figure 4. The two results are consistent with each other in spite of the difference in the focal mechanism. A linear regression analysis is carried out between $\log M_0$ and $\log f_0$ for the all events in Figure 4 and

$$M_0 \propto f_0^{-3.3 \pm 0.2} \qquad (5)$$

is obtained as shown by the dashed line in Figure 4.

4. Discussion and Conclusion

[15] According to *Ide and Beroza* [2001], *Ide* [2003] and *Yamada et al.* [2005], $\tilde{e}$ is almost constant between 10^{-6} and 10^{-4} over a wide moment range from micro earthquakes in gold mine ($M_0 \sim 10^4$ Nm) to great earthquakes in subduction zone ($M_0 \sim 10^{21}$ Nm). On the other hand, *Kanamori et al.* [1993], *Abercrombie* [1995], *Mayeda and Walter* [1996], *Izutani and Kanamori* [2001], *Mori et al.* [2003], and *Mayeda et al.* [2005] pointed out that $\tilde{e}$ is scale-dependent for earthquakes in southern California and in Japan. Although $\tilde{e}$ obtained in the present study is located just in the middle of the scatter by *Ide and Beroza* [2001], $\tilde{e}$ is not constant but increases with the event size.

[16] *Mayeda et al.* [2005] obtained least square lines between $\log \tilde{e}$ and $\log M_0$ for four large earthquakes and their aftershocks. The slope, m, of the line is 0.176 ± 0.05 for the Hector Mine earthquake and its aftershocks and

Figure 3. Seismic energy-to-moment ratio, $\tilde{e}$, as a function of M_w. *Izutani and Kanamori* [2001] is the result for shallow strike-slip earthquakes in the south-western part of Japan.
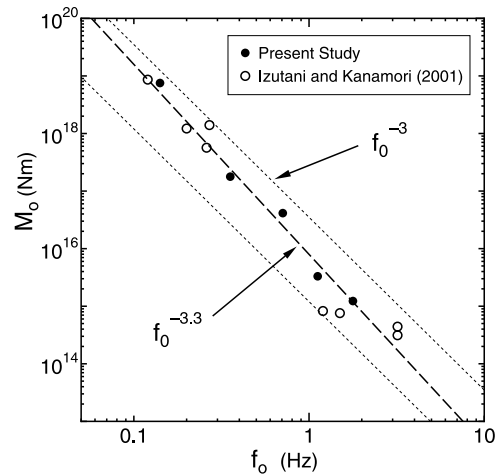
0.164 ± 0.05 for the Landers earthquake and its aftershocks. The slope, m, for the present result is obtained as $0.15 ± 0.2$ by the least squares fitting, which is very close to the slope for the Hector Mine and the Landers earthquakes. Collecting $\tilde{e}$ for earthquakes in various tectonic environments [e.g., *Ide and Beroza*, 2001] apparently shows constant $\tilde{e}$ with very large scatter. However, $\tilde{e}$ for a suite of events in a specific tectonic region definitely shows scale-dependence.

[17] *Kanamori and Rivera* [2004] discussed on the physical meaning of the scale-dependence of $\tilde{e}$. Based on physical consideration, they presented a relationship between M_0 and f_0 as

$$M_0 \propto \left(\Delta\sigma_s V^3\right) f_0^{-3}, \qquad (6)$$

where $\Delta\sigma_s$ is the static stress drop and V is the rupture velocity. The present result of Equation (5) suggests

$$\Delta\sigma_s V^3 \propto f_0^{-0.3} \propto M_0^{0.3/3.3}. \qquad (7)$$

Since the ratio of M_0 between Event 1 and Event 5 is about 10^4, the ratio of $\Delta\sigma_s V^3$ is expected to be about 2.5. The difference in $\Delta\sigma_s V^3$ is sometimes interpreted as the difference in $\Delta\sigma_s$ based on the assumption of constant V. Then, the scale-dependence of $\tilde{e}$ is merely attributed to the scale-dependence of $\Delta\sigma_s$, that is, $\Delta\sigma_s$ of smaller earthquakes is smaller than that of larger earthquakes [e.g., *Beeler et al.*, 2003]. However, it would be natural to think that V and $\Delta\sigma_s$ interrelate with each other. *Kanamori and Rivera* [2004] suggest a possibility that $\Delta\sigma_s$ of smaller earthquakes is larger than that of larger earthquakes and V of smaller earthquakes is smaller than that of larger earthquakes.

[18] The present results, 1) source spectral ratio obtained from the records is inconsistent with that expected from the self-similar omega-square model, 2) $\tilde{e}$ is scale-dependent, and 3) $M_0 \propto f_0^{-3.3\pm0.2}$, suggest a break in self-similarity. To do further discussion on the physical meaning of the break in self-similarity, it is necessary to evaluate $\Delta\sigma_s$ and V independently.

References

Abercrombie, R. E. (1995), Earthquake source scaling relationship from −1 to 5 using seismograms recorded at 2.5-km depth, *J. Geophys. Res.*, *100*, 24,015–24,036.

Aki, K. (1967), Scaling law of seismic spectrum, *J. Geophys. Res.*, *72*, 1217–1231.

Beeler, N. M., T.-F. Wong, and S. H. Hickman (2003), On the expected relationship among apparent stress, static stress drop, effective shear fracture energy, and efficiency, *Bull. Seismol. Soc. Am.*, *93*, 1381–1389.

Brune, J. N. (1970), Tectonic stress and spectra of seismic shear waves from earthquakes, *J. Geophys. Res.*, *75*, 4997–5009.

Hough, S. E., and H. Kanamori (2001), Source properties of earthquakes near the Salton Sea triggered by the 10/16/1999 M7.1 Hector Mine earthquake, *Bull. Seismol. Soc. Am.*, *91*, 456–467.

Ide, S. (2003), Apparent break in earthquake scaling due to path and site effects on deep borehole recordings, *J. Geophys. Res.*, *108*(B5), 2271, doi:10.1029/2001JB001617.

Ide, S., and G. C. Beroza (2001), Does apparent stress vary with earthquake size?, *Geophys. Res. Lett.*, *28*, 3349–3352.

Izutani, Y. (2004), Nonlinear response of surface layers at KiK-net stations in Japan, paper presented at 13th World Conference on Earthquake Engineering, Int. Assoc. of Earthquake Eng., Vancouver, B. C., Canada.

Izutani, Y., and H. Kanamori (2001), Scale dependence of seismic energy-to-moment ratio for strike-slip earthquakes in Japan, *Geophys. Res. Lett.*, *28*, 4007–4010.

Kanamori, H., and L. Rivera (2004), Static and dynamic scaling relations for earthquakes and their implications for rupture speed and stress drop, *Bull. Seismol. Soc. Am.*, *94*, 314–319.

Kanamori, H., E. Hauksson, L. K. Hutton, and L. M. Jones (1993), Determination of earthquake energy release and ML using TERRAscope, *Bull. Seismol. Soc. Am.*, *83*, 330–346.

Mayeda, K., and W. R. Walter (1996), Moment, energy, stress drop, and source spectra of western United States earthquakes from regional coda envelopes, *J. Geophys. Res.*, *101*, 11,195–11,208.

Mayeda, K., R. Gök, W. R. Walter, and A. Hofstetter (2005), Evidence for non-constant energy/moment scaling from coda-derived source spectra, *Geophys. Res. Lett.*, *32*, L10306, doi:10.1029/2005GL022405.

Mori, J., R. E. Abercrombie, and H. Kanamori (2003), Stress drops and radiated energy of aftershocks of the 1994 Northridge, California, earthquake, *J. Geophys. Res.*, *108*(B11), 2545, doi:10.1029/2001JB000474.

Venkataraman, A., L. Rivera, and H. Kanamori (2002), Radiated energy from the October 16, 1999 Hector Mine Earthquake: Regional and teleseismic estimates, *Bull. Seismol. Soc. Am.*, *92*, 1256–1265.

Yamada, T., J. J. Mori, S. Ide, H. Kawakata, Y. Iio, and H. Ogasawara (2005), Radiation efficiency and apparent stress of small earthquakes in a South African gold mine, *J. Geophys. Res.*, *110*, B01305, doi:10.1029/2004JB003221.

_____

Y. Izutani, Department of Civil Engineering, Shinshu University, 4-17-1 Wakasato, Nagano 380-8553, Japan. (tdp0000@gipwc.shinshu-u.ac.jp)